

## Coulomb collisions in strong magnetic fields

Guy Miller and Ira Wasserman

*Center for Radiophysics and Space Research, Cornell University, Ithaca, New York 14853*

(Received 25 January 1984; revised manuscript received 20 June 1984)

Integrated moments of the transition matrix elements for proton-electron Coulomb collisions in strong ( $B \geq 10^{12}$  G) magnetic fields are calculated numerically. Calculations are carried out for various energies and incident angles. Excitations of the electrons to the first excited Landau level are included. Analytic results are also presented for comparison. These calculations should be applicable to detailed models for the x-ray emission from accreting, magnetized neutron stars.

## I. INTRODUCTION

In modeling the emergent x-ray spectrum from an accreting neutron star, a detailed evaluation of the deposition of energy and momentum by the infalling material in the stellar atmosphere is crucial. For the special case of accretion onto a neutron star with no surface magnetic field  $B$ , two distinct types of models for the deceleration of infalling material have been considered. In the first type of model, accreting material is slowed down collisionally as it penetrates the neutron star's atmosphere, the dominant scattering process being Coulomb collisions.<sup>1,2</sup> In the second type of model, collective (plasma) effects slow accreting material more efficiently than any collisional process.<sup>1,3</sup> If the deceleration due to collective effects is extremely rapid, a standing shock may form just above the stellar surface and the kinetic energy of the incident stream is quickly randomized in the vicinity of the collisionless shock.<sup>3</sup>

Recent observations of cyclotron features in the spectra of pulsating x-ray sources<sup>4-8</sup> underscore the importance of the more general (and interesting) case of accretion onto a magnetic neutron star,  $B \neq 0$ . Once again, both collisional and collisionless deceleration models can be considered. In this paper we will focus our attention on *collisional* deceleration via Coulomb collisions of accreting protons with atmospheric electrons.<sup>9,10</sup> Specifically, we present numerical results for various integrated moments of the transition rate for Coulomb collisions in a strong magnetic field. These quantities allow, for example, the calculation of friction coefficients in the Fokker-Planck equation for the incident proton beam, and should be useful in simulating the deceleration of accreting material.

The calculations presented in this paper have, we feel, several advantages over previous work. First, the phase-space restrictions on the momentum transfer and the proton recoil have been properly treated for arbitrary "pitch angle" between the proton momentum and magnetic axis. This results in values of the friction and diffusion coefficients which are reliable at arbitrary pitch angle, in contrast to previous work (cf. Ventura,<sup>11</sup> Pavlov and Yakovlev,<sup>12</sup> and Langer<sup>12</sup>). Second, no restriction to very small momentum transfer is made (cf. Kirk and Gallo-way<sup>13</sup>). This improvement affects *all* of the quantities we calculate, but is, in particular, crucial to a reliable evalua-

tion of the excitation cross sections. Third, we do not average our results over an assumed electron-velocity distribution, so that the moments calculated here should be useful for a variety of applications, involving both thermal and nonthermal electrons. The calculated moments can be implemented in a straightforward way in a Monte Carlo calculation of the stopping length of accreting protons. We shall report on the results of such a calculation in a future paper.<sup>24</sup>

In Sec. II we review the physical conditions in the atmosphere of an accreting magnetic neutron star, and list the approximations used in our computations. Basic equations for the calculated integrals are given in Sec. III, where our numerical methods are also discussed. As the work involved numerical phase-space integrals of differential rates, we also present analytic estimates of the integrals in different limiting regimes for comparison with the numerical results. Numerical results and conclusions are given in Sec. IV.

## II. PHYSICAL CONDITIONS AND APPROXIMATIONS

Electrons in a spatially uniform magnetic field are described quantum mechanically by Landau wave functions. A given electronic state has total energy (nonrelativistic)

$$E = \frac{p^2}{2m_e} + (n + \frac{1}{2})\hbar\omega_c, \quad (1)$$

where  $\omega_c = eB/(m_e c)$  is the electron gyrofrequency,  $p$  is the electron momentum along the magnetic field axis, and  $n$ , which characterizes the kinetic energy perpendicular to the field, is a non-negative integer.<sup>14</sup> In the atmosphere of an accreting x-ray source, which may not be in strict thermodynamic equilibrium, we can therefore distinguish three different energy scales for the electrons:  $k_B T_{||}$ , the typical kinetic energy along the field,  $k_B T_{\perp}$ , the typical transverse kinetic energy, and  $\hbar\omega_c \approx 11.6 B_{12}$  keV, where  $B_{12} \equiv B/(10^{12}$  G). Typically,  $k_B T_{||} \sim 10$  keV for x-ray pulsars<sup>15</sup> and, since the rate of collisional excitations in the course of Coulomb collisions among atmospheric elec-

trons and ions is slow<sup>11,16</sup> in comparison with the radiative deexcitation rate, we expect  $T_{\perp} \lesssim T_{\parallel}$ . Thus, for  $B_{12} \sim 1$  (which is characteristic, for example, of radiopulsars<sup>17</sup>) we expect  $k_B T_{\perp} \lesssim \hbar\omega_c$ , and perhaps  $k_B T_{\perp} \ll \hbar\omega_c$ . For Her X-1, the best-studied x-ray pulsar, the observed cyclotron features<sup>4-6,8</sup> imply  $\hbar\omega_c \approx 40-50$  keV (corresponding to  $B_{12} \approx 3.4-4.3$ ) so that  $k_B T_{\perp} \leq 0.2\hbar\omega_c$  in our calculations. Thus to a good approximation essentially all atmospheric electrons are in the ground state.

Accreting protons free-fall onto the stellar surface with a speed  $v_{ff} = (2GM/R)^{1/2} \approx 0.54c$  for a neutron star with mass  $M \approx 1M_{\odot}$  and radius  $R \approx 10$  km. Since  $m_e v_{ff}^2/2 = GMm_e/R \approx 75$  keV, collisional excitation of  $n=0$  atmospheric electrons in "knock-on" collisions is possible. However, in the cases of interest, collisional excitations should be confined to low-lying Landau levels. For example, when  $B_{12} \gtrsim 3$  (as is the case for Her X-1) excitations to the  $n=1$  state should dominate. In the following, we consider only collisions for which either the atmospheric electron remains in the ground state ( $0 \rightarrow 0$  transitions), or is knocked into the first excited state ( $0 \rightarrow 1$  transitions). Our numerical work can be extended easily to include higher excitations.

In computing collision matrix elements we employ the Born approximation, and adopt plane-wave states for the accreting protons, but use exact Landau wave functions for the electrons. Protons and electrons are treated nonrelativistically. Even though  $v_{ff} \approx 0.54c$  for the protons as they impinge on the atmosphere, the kinematic effects of the nonrelativistic approximation should not be important, and time-dilation effects should only lead to errors  $\sim \frac{1}{2}(v_{ff}/c)^2 \approx 15\%$ . The interaction potential is taken to be a statically screened Coulomb potential

$$V(\vec{r}_e - \vec{r}_i) = -e^2 \frac{\exp(-\kappa_s |\vec{r}_e - \vec{r}_i|)}{|\vec{r}_e - \vec{r}_i|} \quad (2)$$

for a proton at position  $\vec{r}_i$  and an electron at position  $\vec{r}_e$ . The screening length  $\kappa_s^{-1}$  is an arbitrary parameter in our calculations, but it is expected<sup>11,18</sup> that  $\kappa_s \sim \kappa_D$ , where the Debye length in the absence of a magnetic field is

$$\begin{aligned} \kappa_D^{-1} &= (k_B T_{\parallel} / 4\pi n_e e^2)^{1/2} \\ &= 2.4 \times 10^{-7} [k_B T_{\parallel} / (10 \text{ keV})]^{1/2} \\ &\quad \times [n_e / (10^{23} \text{ cm}^{-3})]^{-1/2} \text{ cm} \end{aligned} \quad (3)$$

for an atmospheric electron density  $n_e$  and temperature  $T_{\parallel}$ . Two possible refinements to the choice  $\kappa_s \equiv \kappa_D$  should be noted. First, our use of plane-wave states for the proton represents a classical approximation in which we ignore the fact that the proton actually has Landau levels like the electron. The minimum momentum transfer needed to change the proton's Landau level has an associated length

$$\begin{aligned} \kappa_g^{-1} &= (m_p / m_e) v / \omega_c \\ &= 3.1 \times 10^{-6} \left[ \frac{v}{c} \right] B_{12}^{-1} \text{ cm}, \end{aligned} \quad (4)$$

where  $v$  is the proton speed in the Galilean frame in which the electron initially has no velocity along the field.

If  $\kappa_g^{-1}$  is smaller than the Debye length, the use of plane-wave proton wave functions is inaccurate for low-momentum transfer,  $\kappa \lesssim \kappa_g$ . As will be apparent in Sec. III this inaccuracy only affects the Coulomb logarithm, so we should be able to take  $\kappa_s = \kappa_g$  in this case, making only a (small) logarithmic error. Second, because  $(k_B T_{\parallel} / m_e)^{1/2} \approx 0.14 [k_B T_{\parallel} / (10 \text{ keV})]^{1/2} c$  is somewhat smaller than the typical proton speed  $v_{ff} \approx 0.54c$ , we should in principle use a dynamically screened interaction potential in computing matrix elements.<sup>19</sup> Once again the resulting error should appear only in the Coulomb logarithm, and can be roughly taken into account by taking

$$\kappa_s = [4\pi n_e e^2 / (\frac{1}{2} m_e v_{ff}^2)]^{1/2}.$$

### III. CALCULATION OF MATRIX ELEMENTS AND INTEGRATED MOMENTS

#### A. General Overview and Choice of Natural Units

The Fokker-Planck (FP) equation can be used to follow changes in the proton distribution function caused by collisions provided the momentum transfer per scatter is sufficiently small. However, transport coefficients involving integrals of the linear and quadratic moments of the momentum transfer weighted by the differential collision rate must be computed before the FP equation can be solved.<sup>20</sup> Therefore, to determine these coefficients one must have an expression for the differential collision rate which, when multiplied by the appropriate moments of momentum transfer, may be analytically or numerically integrated over the kinematically allowed phase space for all collisions.

The differential collision rate was calculated using the distorted-wave Born approximation,

$$d\Gamma(i \rightarrow f) = \frac{2\pi}{\hbar} |\langle f | H_{\text{int}} | i \rangle|^2 \delta(E_f - E_i) df, \quad (5)$$

where  $H_{\text{int}}$  is the interaction Hamiltonian,  $i$  indicates the initial state of both the electron and the interloping proton,  $f$  the final state,  $E_a$  is the energy of state  $a$ , and  $df$  denotes the final-state phase-space element. As was mentioned in Sec. II, protons are described by plane-wave states, for which the wave functions are

$$\psi_i(\vec{r}_i) = L^{-3/2} \exp(i \vec{k}_i \cdot \vec{r}_i) \quad (6)$$

for momentum  $\hbar \vec{k}_i$  and normalization volume  $V = L^3$ . The electron wave functions are taken to be<sup>14</sup>

$$\begin{aligned} \psi_e(\vec{r}_e) &= (2\pi L)^{-1/2} \exp\{i[k_z z_e + (n-s)\phi_e]\} \\ &\quad \times \left[ \lambda^{-1} I_{ns} \left[ \frac{1}{2} \rho_e^2 \frac{eB}{\hbar c} \right] \right] \end{aligned} \quad (7)$$

in cylindrical coordinates  $(\rho_e, \phi_e, z_e)$ , with

$$I_{ns}(z) = (-1)^s (s! / n!)^{1/2} z^{(n-s)/2} e^{-z/2} L_s^{n-s}(z), \quad (8)$$

where  $L_{\alpha}^{\beta}(z)$  is the generalized LaGuerre polynomial.<sup>21</sup> The total energy of this electronic state is given by Eq. (1) with  $p = \hbar k_z$  and  $s$  is a degenerate quantum number.

For the Landau wave functions, a natural unit of length is [cf. Eq. (7)]

$$\begin{aligned}\lambda &\equiv (\hbar/\omega_c m_e)^{1/2} \\ &= 2.56 \times 10^{-10} B_{12}^{-1/2} \text{ cm}\end{aligned}\quad (9)$$

and the natural unit of momentum is

$$\begin{aligned}p_B &= \hbar/\lambda = (\hbar\omega_c m_e)^{1/2} \\ &= 4.10 \times 10^{-18} B_{12}^{1/2} \text{ g cm s}^{-1}.\end{aligned}\quad (10)$$

In the following, all momenta will be expressed in units of  $p_B$ . A natural unit of velocity is

$$\begin{aligned}v_B &= p_B/m_e \\ &= 4.50 \times 10^9 B_{12}^{1/2} \text{ cm s}^{-1}\end{aligned}\quad (11)$$

or equivalently,

$$v_B = c(B/B_c)^{1/2}\quad (12)$$

where

$$\begin{aligned}B_c &= m_e^2 c^3 / e \hbar \\ &= 4.41 \times 10^{13} \text{ G}.\end{aligned}\quad (13)$$

Physically, we may think of our unit of length as being roughly the size of the smallest Landau orbit. Our unit of velocity is then seen to be the typical speed of an electron in such an orbit. Energy transfers will be expressed in terms of the Landau-level spacing,  $\hbar\omega_c = 11.6 B_{12}$  keV. Thus, for an electron at rest and a proton moving straight down along the field at a speed  $v = uv_B$ , Coulomb excitation to the  $n$ th electronic Landau level is possible only if  $u^2 > 2n$ , in our units.

### B. Matrix Elements

In our system of units the Coulomb interaction Hamiltonian for proton-electron scattering is

$$H_{\text{int}}(\vec{r}_e - \vec{r}_i) = -\alpha_e (B/B_c)^{-1/2} \frac{\exp(-\kappa_s |\vec{r}_e - \vec{r}_i|)}{|\vec{r}_e - \vec{r}_i|}\quad (14)$$

where  $\alpha_e = e^2/\hbar c$ . The momentum  $\vec{q}$  with components  $x$  and  $y$  perpendicular to the magnetic axis and  $q_{\parallel}$  along the field is transferred from the incident proton to the atmospheric target electron in each Coulomb collision. We adopt  $L^3 = n_e^{-1}$ , where  $n_e$  is the (dimensionless) atmospheric electron number density, so that the reaction rate [Eq. (5)] is the differential rate per incident proton of scattering events with momentum transfer  $\vec{q}$ . After summing on the final value of the degenerate electron quantum number  $s$ , and averaging over its initial value we get<sup>22</sup>

$$\begin{aligned}d\Gamma_{nn'}(\vec{q}) &= [4\alpha_e^2 n_e (B/B_c)^{-1}] \frac{I_{nn'}^2(\frac{1}{2}(x^2 + y^2))}{(x^2 + y^2 + q_{\parallel}^2 + \kappa_s^2)^2} \\ &\quad \times \delta(E_f - E_i) dx dy dq_{\parallel}\end{aligned}\quad (15)$$

for an electron initially in the  $n$ th and finally in the  $n'$ th Landau state. Here  $I_{nn'}(z)$  is given by Eq. (8) with  $s = n'$ .

To find the rate of scattering from one proton state to another due to scatterings in an actual atmosphere, we also have to average the differential rate over the distribution of electron quantum numbers  $n$  and  $k_z$  in the initial state. As was discussed in Sec. II, we assume that  $n=0$  only for atmospheric electrons. Because of Galilean invariance along the field only the *relative* velocity of the electron and proton parallel to  $\vec{B}$  enters the rate; neither  $z$  component occurs independently. Thus, in our calculation of a differential rate of scattering from an initial state with momentum  $(m_p/m_e)\vec{u}$  with components  $(m_p/m_e)(u \sin\theta, 0, u \cos\theta)$  to a final state of momentum  $(m_p/m_e)\vec{u} - \vec{q}$ , we need calculate only the rate for an initially stationary electron  $k_{z,i} = 0$  for different values of  $\vec{u}$ . The rate with a thermal distribution of electron velocities along the field—or any other distribution—may then be derived by integrating over the appropriate range of relative velocities. Specifically, if we know the differential rate of collisions  $d\Gamma(\vec{u}, \vec{q})$  with momentum transfer  $\vec{q}$  starting with a proton of velocity  $\vec{u}$  and a stationary electron, and we wish to find a rate  $d\Gamma_{\text{new}}(\vec{u}, \vec{q})$  for similar collisions with an initial distribution of electron momentum  $f(k_{z,i})$ , we have

$$d\Gamma_{\text{new}}(\vec{u}, \vec{q}) = \int d\Gamma(\vec{u} - k_{z,i} \hat{e}_z, \vec{q}) f(k_{z,i}) dk_{z,i}.\quad (16)$$

### C. Phase space

Next, we consider the structure of the phase space over which the above integrals should be taken. The allowed transitions are determined by conservation of energy for a given momentum transfer  $\vec{q}$ . If  $k_z = 0$  initially, then in our system of units

$$E_f - E_i = \frac{1}{2} \left[ q_{\parallel}^2 - 2\vec{u} \cdot \vec{q} + \frac{m_e}{m_p} (x^2 + y^2) + 2(n' - n) \right]\quad (17)$$

for an  $n$  to  $n'$  transition. The integrals we must do over the three-dimensional space of momentum transfer than may be immediately reduced to two-dimensional integrals by integrating in one dimension over the energy-conserving  $\delta$  function. We are thus left with two-dimensional integrals which must be done numerically. A little insight into the numerical technique and methods of approximation may be gained if we make some simple observations regarding the shape of the surface  $E_f - E_i = 0$  in the original three-dimensional space before we present the two-dimensional forms of the integrals. First, the surface is an oblate spheroid; its principal axis in the  $q_{\parallel}$  direction is  $(m_e/m_p)^{1/2}$  times shorter than the  $x$ - and  $y$ -principal axes. Second, regardless of the particular transition, all spheroids are centered at the same point  $[(m_p/m_e)u \sin\theta, 0, u \cos\theta]$ , and spheroids with a larger  $\Delta n = n' - n$  are nested within spheroids of smaller  $\Delta n$ . In particular, the  $\Delta n = 0$  spheroid encloses all the others, and it is always tangent to the origin. With this in mind, let us consider how this spheroid changes with changing an-

gle  $\theta$ , at a given velocity  $u$ . When  $\theta=0$  (i.e., the incident proton is moving along the field), the spheroid is tangent to the  $x$ - $y$  plane at the origin. As  $\theta$  increases to  $\pi/2$ , the spheroid grows rapidly in size, as its center moves out in the  $x$  direction and simultaneously descends onto the  $x$ - $y$  plane. It lies wholly in the region  $x > 0$  when  $\theta = \pi/2$ , being tangent to the  $y$ - $q_{\parallel}$  plane. This shows why, near  $\theta = \pi/2$ ,  $y$  and  $q_{\parallel}$  are a convenient pair of integration variables, whereas for smaller angles  $x$  and  $y$  are the best choices. If we use the energy-conserving  $\delta$  function to integrate over  $q_{\parallel}$ , we are left with integrals over  $x$  and  $y$ . Linear moments of the transition rate are proportional to

$$I_{\alpha}^{nn'}(u, \theta) = \sum_{l=+,-} \int \int \frac{\alpha I_{nn'}^2 \left[ \frac{x^2 + y^2}{2} \right]}{(x^2 + y^2 + (q_{\parallel}^l)^2 + \kappa_s^2)^2 k_r} dx dy \quad (18)$$

and the quadratic moments are proportional to

$$I_{\alpha\beta}^{nn'}(u, \theta) = \sum_{l=+,-} \int \int \frac{\alpha\beta I_{nn'}^2 \left[ \frac{x^2 + y^2}{2} \right]}{(x^2 + y^2 + (q_{\parallel}^l)^2 + \kappa_s^2)^2 k_r} dx dy \quad (19)$$

where  $\alpha, \beta \in \{x, y, q_{\parallel}^{\pm}\}$ , and

$$q_{\parallel}^{\pm} = u \cos\theta \pm k_r \quad (20)$$

with

$$k_r = \left[ u^2 \cos^2\theta + 2ux \sin\theta - 2(n' - n) - \frac{m_e}{m_p} (x^2 + y^2) \right]^{1/2}. \quad (21)$$

The rate of collisional excitations from  $n=0$  to  $n'=1$  is similarly proportional to

$$I^{01}(u, \theta) = \sum_{l=+,-} \int \int \frac{I_{01}^2 \left[ \frac{x^2 + y^2}{2} \right]}{[x^2 + y^2 + (q_{\parallel}^l)^2 + \kappa_s^2]^2 k_r} dx dy \quad (22)$$

for a given proton velocity. The constant of proportionality in all cases is  $4\alpha_e^2 n_e (B/B_c)^{-1}$  times the (suitably transformed) electron distribution function.

#### D. Numerical Evaluation of the Phase-Space Integrals

The integrals in Eqs. (18), (19), and (22) have been evaluated with  $n=0$  but  $n'=0$  or 1, and  $0.1 \leq u \leq 33$  for all angles (except in the case of some contributions from the  $0 \rightarrow 1$  transitions, which become very small by the time  $u=0.5$ ). The numerical integrations were done using the provisional value  $\kappa_s^2 = 10^{-6}$ . We provide formulas which have been checked by further numerical integrations to extrapolate these results to different values of  $\kappa_s^2$ .

Several problems brought about by the nature of the integrands must be addressed in numerically obtaining the

integrals. The first problem comes from the quantity  $k_r$  in the denominators. The projected area of integration is a disk in the  $x$ - $y$  plane on the perimeter of which  $k_r$  goes to zero. The integrand then becomes singular, but of course the integral is not. This problem was solved by omitting a very narrow ring from the region of integration at the edge of the disk. This ring makes a negligibly small contribution to our integrals until  $\theta$  is nearly  $\pi/2$ . At such high angles, however, we obtain our integrals from a program using  $y$  and  $q_{\parallel}$  as integration variables.

The next problem is that integrands such as that of  $I_x^{00}(u, \theta)$  are nearly antisymmetric in  $x$  near the origin, while large contributions to the integrals come from that neighborhood. To avoid near cancellation of large terms, we integrated the symmetrized integrand

$$f_s(x, y) = f(x, y) + f(-x, y) \quad (23)$$

over that part of the disk of integration with  $x > 0$  which as a counterpart with  $x < 0$  (see Fig. 1). Note that all our integrands (with the exception of those in  $I_y^{nn'}$  and  $I_{y\alpha}^{nn'}$ ,  $\alpha \neq y$ , which are identically zero) are even in  $y$ , so we integrated only over  $y \leq 0$ , doubling the value at the end of the numerical integration to obtain the correct result.

The last problem arising is peculiar to the  $\Delta n = 0$  integrals with  $\kappa_s^2 \ll 1$ , for which the two-dimensional integrals are logarithmically divergent. In this case, the integrand is sharply peaked near the origin, making the numerical integration time consuming. We therefore found functions which matched the integrands very closely at the origin, and which could be integrated analytically over a small, semielliptical patch centered on the origin and lying well within the region of integration. These functions were subtracted from the integrands within the patch, and the patch was integrated separately from the rest of the symmetrized region (see Fig. 1). The contribution from

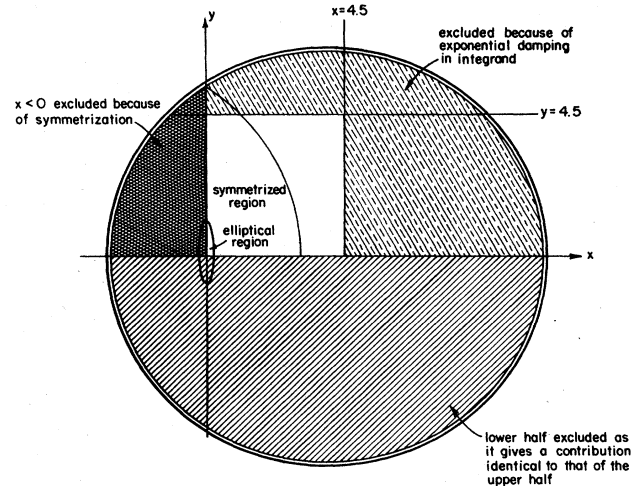


FIG. 1. A diagram of the region of integration as it was subdivided in our integration routine. In the symmetrized region, the symmetrized function  $f(x, y) + f(-x, y)$  was integrated; outside of this  $f(x)$  was the function integrated. In the elliptical region, an analytically integrable function was subtracted from the symmetrized integrand to accelerate the numerical integration.

TABLE I. Symmetries of the integrals.

Integral	Symmetry
$I^{nn'}$	$I(\theta) = I(\pi - \theta)$
$I_x^{nn'}$	$I(\theta) = I(\pi - \theta)$
$I_{q_{  }}^{nn'}$	$I(\theta) = -I(\pi - \theta)$
$I_{xx}^{nn'}$	$I(\theta) = I(\pi - \theta)$
$I_{xq_{  }}^{nn'}$	$I(\theta) = -I(\pi - \theta)$
$I_{q_{  }q_{  }}^{nn'}$	$I(\theta) = I(\pi - \theta)$
$I_{yy}^{nn'}$	$I(\theta) = I(\pi - \theta)$

the different subregions were then added together, and the analytically determined contribution by the subtracted function restored to obtain the value of the integral being sought. In all cases, because of the exponential (damping) factor in all of the integrands, we integrated only over those portions of the disk for which  $|x| \leq 4.5$  and  $|y| \leq 4.5$ . (When  $q_{||}$  and  $y$  were used as variables, the lack of a strong exponential damping in  $q_{||}$  made it necessary to adjust the limits of integration in  $q_{||}$  until a consistent value of the integral being done could be found.)

In order to do the two-dimensional integrations, we wrote the integrals as

$$I = \int_0^{y_{\max}} \left[ \int_{a(y)}^{b(y)} f(x,y) dx \right] dy = \int_0^{y_{\max}} F(y) dy \quad (24)$$

and used an adaptive scheme to do the one-dimensional integrals.

TABLE II. Logarithmically divergent contributions.

Integral	$\Delta I$
$I_x^{00}$	$\frac{\pi}{8u^2} [3 \sin(3\theta) - \sin\theta]$
$I_{q_{  }}^{00}$	$\frac{3\pi}{8u^2} [\cos(3\theta) - \cos\theta]$
$I_{xx}^{00}$	$\frac{-\pi}{2u} [1 + \cos(2\theta)]$
$I_{xq_{  }}^{00}$	$\frac{\pi}{2u} \sin(2\theta)$
$I_{q_{  }q_{  }}^{00}$	$\frac{-\pi}{2u} [1 - \cos(2\theta)]$
$I_{yy}^{00}$	$-\frac{\pi}{u}$

A one-dimensional adaptive integration works by approximating the integral of a function over a given interval in two ways; one approximation will involve evaluating the function at more points and will be finer than the other. (In our case three- and five-point Simpson's-rule estimates were used.) If the two approximations do not agree to within a given error tolerance  $\epsilon$ , the interval attempted is halved, and we attempt the leftmost of the two subintervals. When the two agree, we start over with whatever is left of the original interval. We also keep the absolute value of the difference between the two approximations as an estimate of the error made in accepting a given interval, and sum the error estimates for all the accepted subintervals to obtain an estimate of the total error for the complete integral.

A two-dimensional integration has two sources of error: that which comes from knowing  $F(y)$  imperfectly, and  $\epsilon_y$ ,

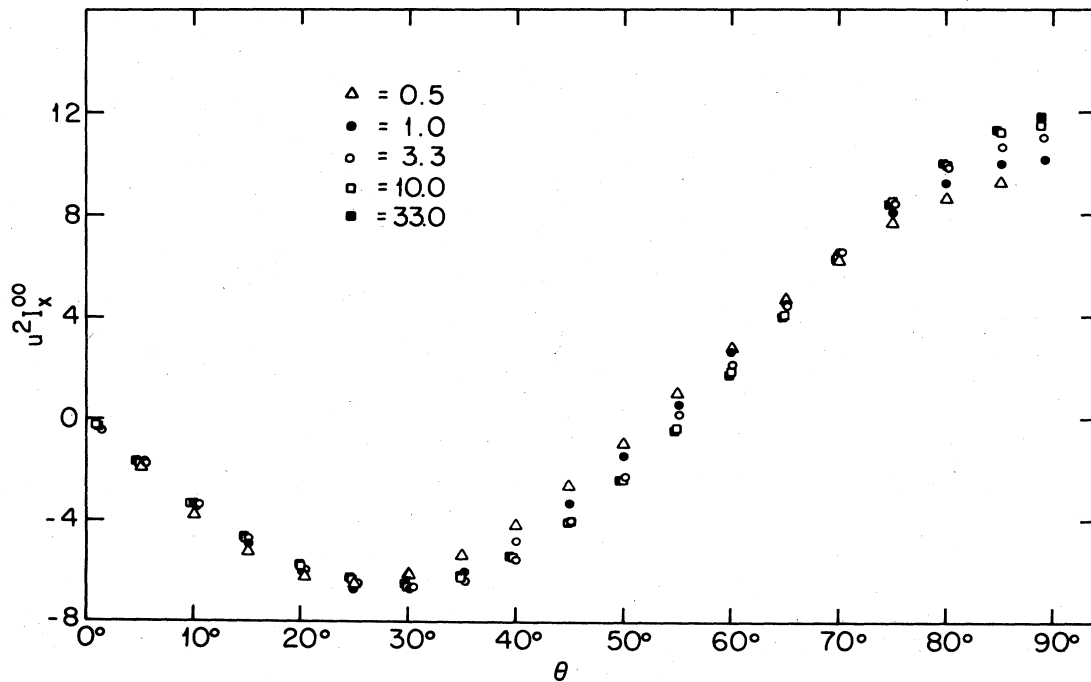


FIG. 2. Plot of linear moment  $I_x^{00}$  multiplied by  $u^2$ , where  $u$  is the dimensionless relative velocity of the electron and proton, as a function of the angle  $\theta$  from the field, for five values of the relative velocity  $u$  (0.5, 1.10, 3.3, 10.0, 33.0).

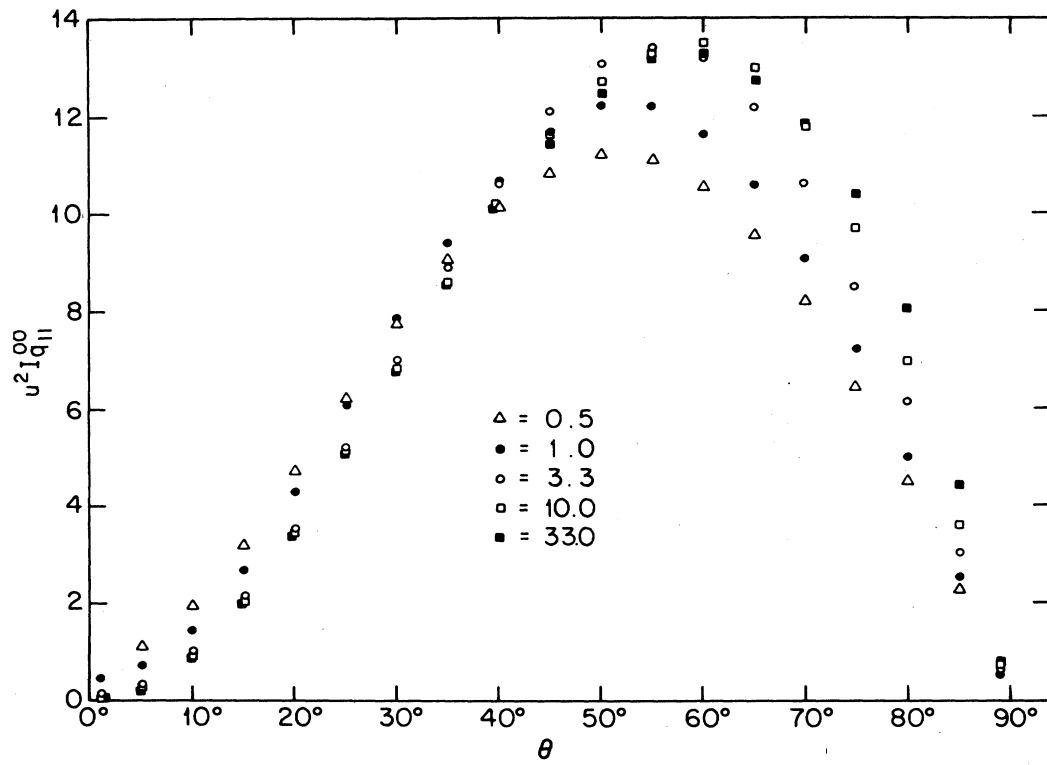


FIG. 3. Plot of the linear moment  $I_{q||}^{00}$  multiplied by  $u^2$ , as a function of  $\theta$  for five values of  $u$ .

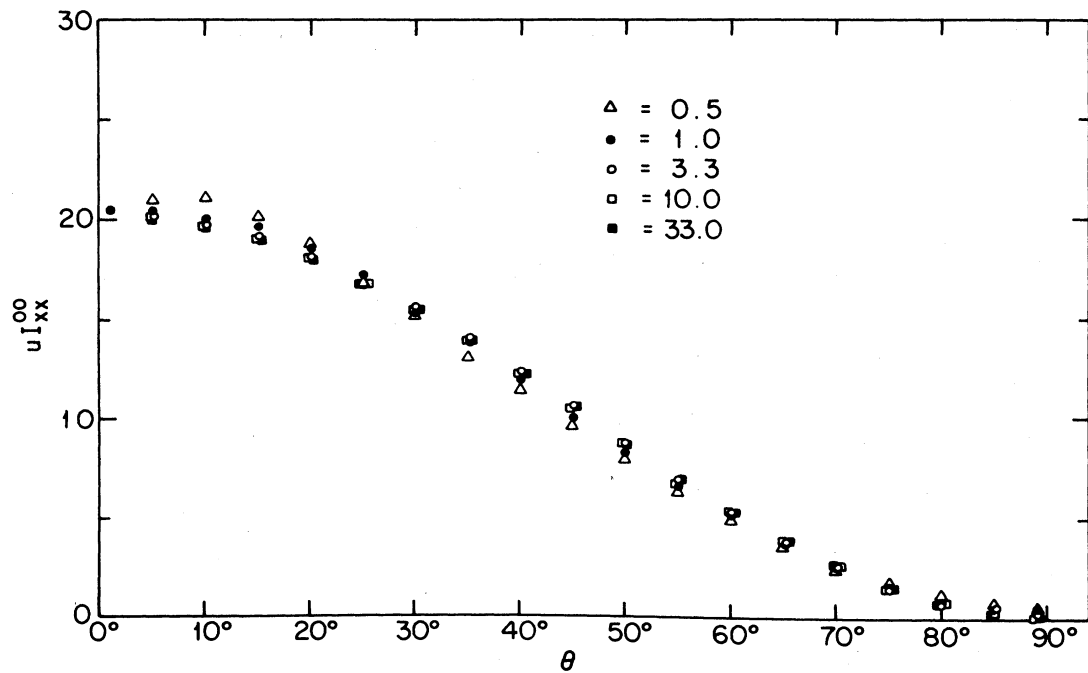


FIG. 4. Plot of the quadratic moment  $I_{xx}^{00}$  multiplied by  $u$ , as a function of  $\theta$  for five values of  $u$ .

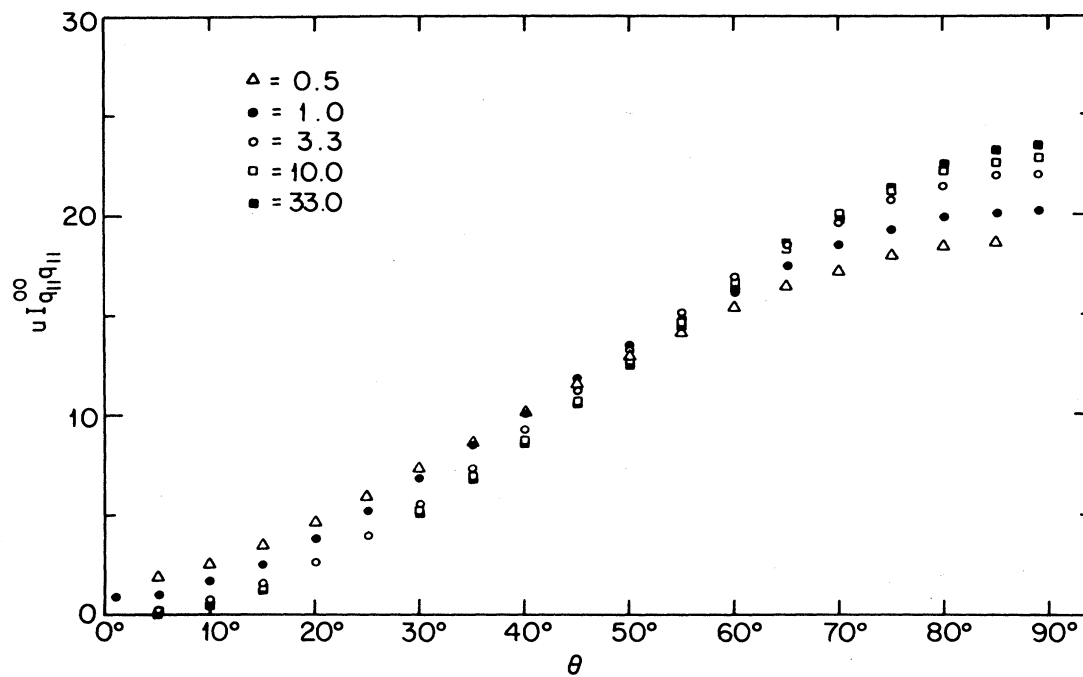


FIG. 5. Plot of the quadratic moment  $I_{q_{||}q_{||}}^{00}$  multiplied by  $u$ , as a function of  $\theta$  for five values of  $u$ .

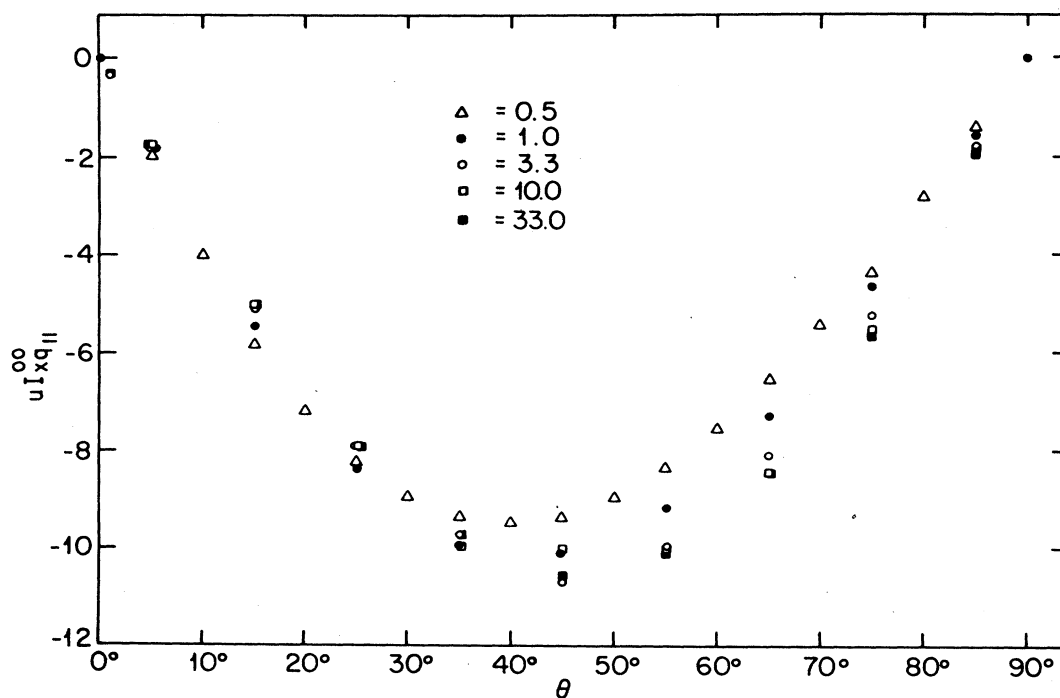


FIG. 6. Plot of the quadratic moment  $I_{xq_{||}}^{00}$  multiplied by  $u$ , as a function of  $\theta$  for five values of  $u$ .

the error which would result from numerically integrating  $F(y)$  even if it were perfectly known (i.e., the contributions from integration in  $x$  and  $y$ , respectively). Choosing the error tolerance  $\epsilon$  appropriately for the  $x$  and  $y$  integrations is crucial. For instance, for 1% accuracy from a given integration over some interval, we might choose  $\epsilon$  to be 0.01 times the five-point estimate. The pitfall of this choice is that one might spend a great deal of effort evaluating very accurately a subinterval which contributes very little to the entire integral. Instead, we include in  $\epsilon$  a small term independent of the subinterval being evaluated, taken to be a tiny fraction of our first estimate of the *entire* integral. We integrate the error in  $F(y)$  with  $y$ , and add to the account being kept of the numerical error resulting solely from integration in  $y$ , thus forming an estimate of the total error in the two-dimensional integration:

$$\epsilon_{\text{tot}} = \int \epsilon_x(y)dy + \epsilon_y. \quad (25)$$

We check that our estimate of the final integral  $I$  is sufficiently accurate by comparing it with  $\epsilon_{\text{tot}}$ . If in doubt, we make another estimate of the integral with a tighter error tolerance, and compare this value with the first. Our estimates of the integrals are nominally good to 1%, except for example, at angles near  $\pi/2$ , where integrals such as  $I_{q_{\parallel}}^{00}$  go to zero and the accuracy performance diminishes.

#### IV. RESULTS AND CONCLUSIONS

Numerical results for  $I_{\alpha}^{00}$ ,  $I_{\alpha\beta}^{00}$ ,  $I_{\alpha}^{01}$ , and  $I_{\alpha\beta}^{01}$  are presented<sup>23</sup> in tables and in Figs. 2–13. The integrals have been computed for  $0 \leq \theta \leq \pi/2$ , and for  $1 \leq u \leq 33$  using the fixed value  $\kappa_s^2 = 10^{-6}$ . The  $0 \rightarrow 0$  transitions also include data for  $u = 0.5$ . Because of the angular symmetries of the various integrals, the tabulated data can easily be applied to a full range of angles  $0 \leq \theta \leq \pi$ . The symmetry of each integral under the transformation  $\theta \rightarrow \pi - \theta$  is given in Table I.

In order to extrapolate from  $\kappa_s^2 = 10^{-6}$  to arbitrary values we write

$$I(\kappa_s^2) = I(\kappa_s^2 = 10^{-6}) + \Delta I \ln(10^3 \kappa_s). \quad (26)$$

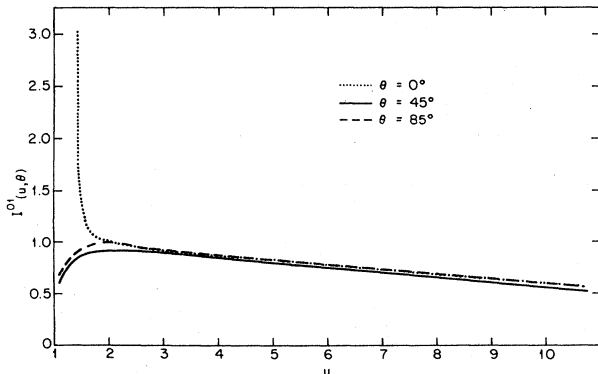


FIG. 7. Plot of the excitation-rate integral  $I^{01}$  as a function of  $u$  for three angles  $\theta$  ( $0^\circ, 45^\circ, 85^\circ$ ).

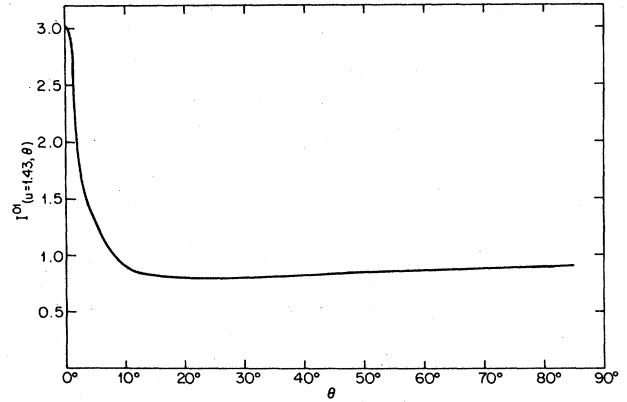


FIG. 8. Plot of  $I^{01}$  for  $u = 1.43$  as a function of angle.

Analytic formulas for  $\Delta I(u, \theta)$  are listed in Table II. Changing  $\kappa_s^2$  only affects integrals for which  $\Delta n = 0$  and there is a logarithmic divergence at small momentum transfers. The formulas for  $\Delta I$  were found for small angles by expanding the integrands in  $x$  and then analytically evaluating the resultant logarithmically divergent integral. To find the  $\kappa_s^2$  contributions for angles near  $\pi/2$  we change integration variables to  $q_{\parallel}$  and  $y$ . We then find expressions for these contributions which are identical to those given by the low-angle formulas in the limit  $\theta \rightarrow \pi/2$ . That the low-angle expressions should be approximately valid for all angles is not too surprising, since the low-angle expansions show that as the angle increases the integrand rapidly grows more sharply peaked in the variable  $x$ . An expansion in  $x$  would therefore not be expected to fail until an angle quite near  $\pi/2$  is reached. The estimates of the *complete* integrals (not just the low momentum transfer contributions) given by these expansions are accurate only for small angles, however. This is because in the Coulomb logarithm there is implicitly a high wave-number cutoff of order unity in addition to the low momentum transfer cutoff  $\sim \kappa_s$ . By this point ( $x \approx 1$ ) the expansion must fail, especially for high angles as the bounds of integration draw within this region and become influential.

To use the data provided in the tables to make models of neutron star atmospheres, one needs to do several things. First, to transform back to conventional units, one must convert the tabulated, dimensionless integrals according to the prescription outlined, in detail, in Appendix A. Second, one needs to take these coefficients and produce from them coefficients appropriate to the velocity distribution of atmospheric electrons in the model under consideration, e.g., a thermal distribution. This is because the quantities we tabulated are for collisions with electrons which are initially at rest along the field: one may view them as being essentially FP coefficients for a cold atmosphere. The invariance of the collision physics under Gallilean transformations along the field [viz. Eq. (16)] allows us to do this very simply. To obtain the moment relevant to a particular distribution of atmospheric electron velocities along the field, we write

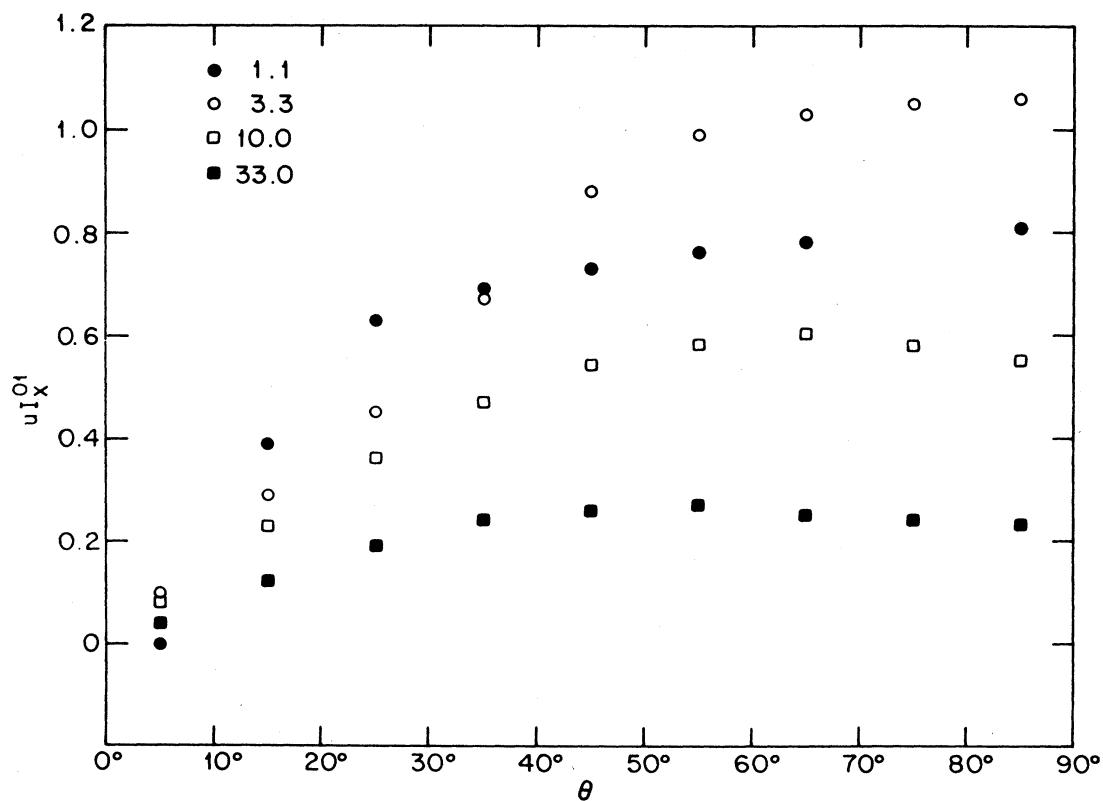


FIG. 9. Plot of the linear moment for the transition  $n=0$  to  $1$ ,  $I_x^{01}$ , multiplied by the relative velocity  $u$ , as a function of the angle  $\theta$  from the field, for four values of  $u$ .

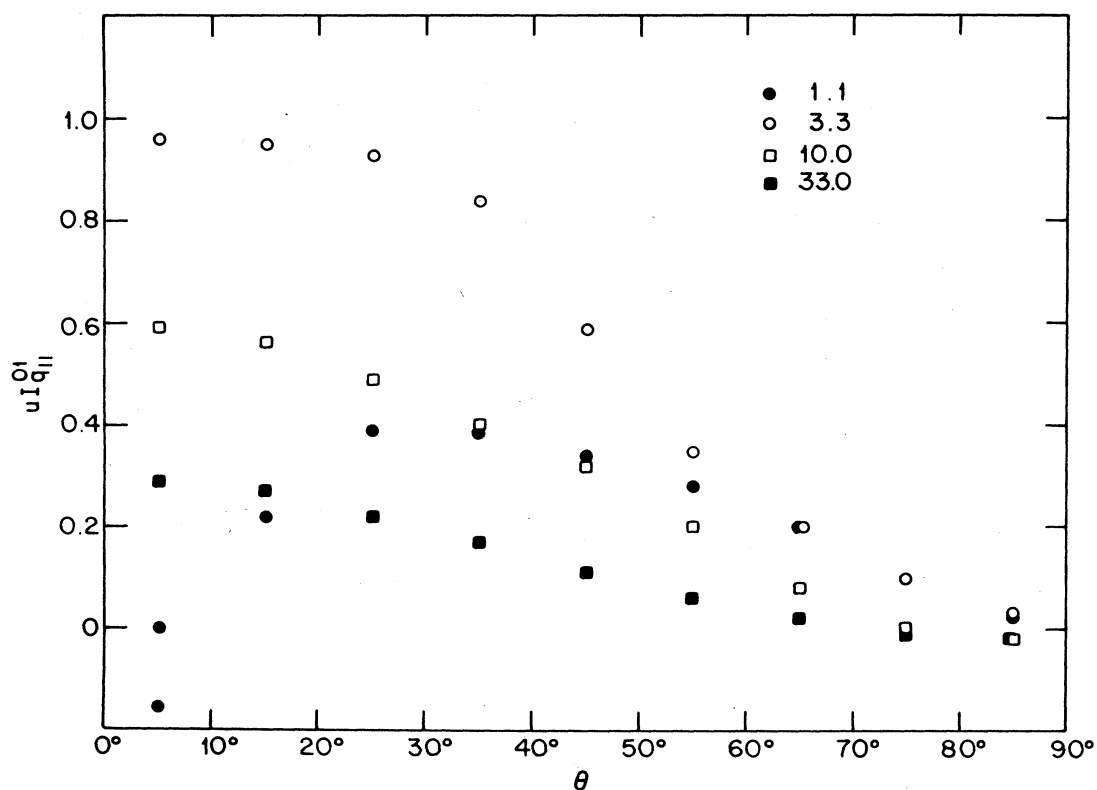


FIG. 10. Plot of the linear moment for  $0 \rightarrow 1$  transitions  $I_{q_{||}}^{01}$ , multiplied by  $u$ , as a function of  $\theta$  for four values of  $u$ .

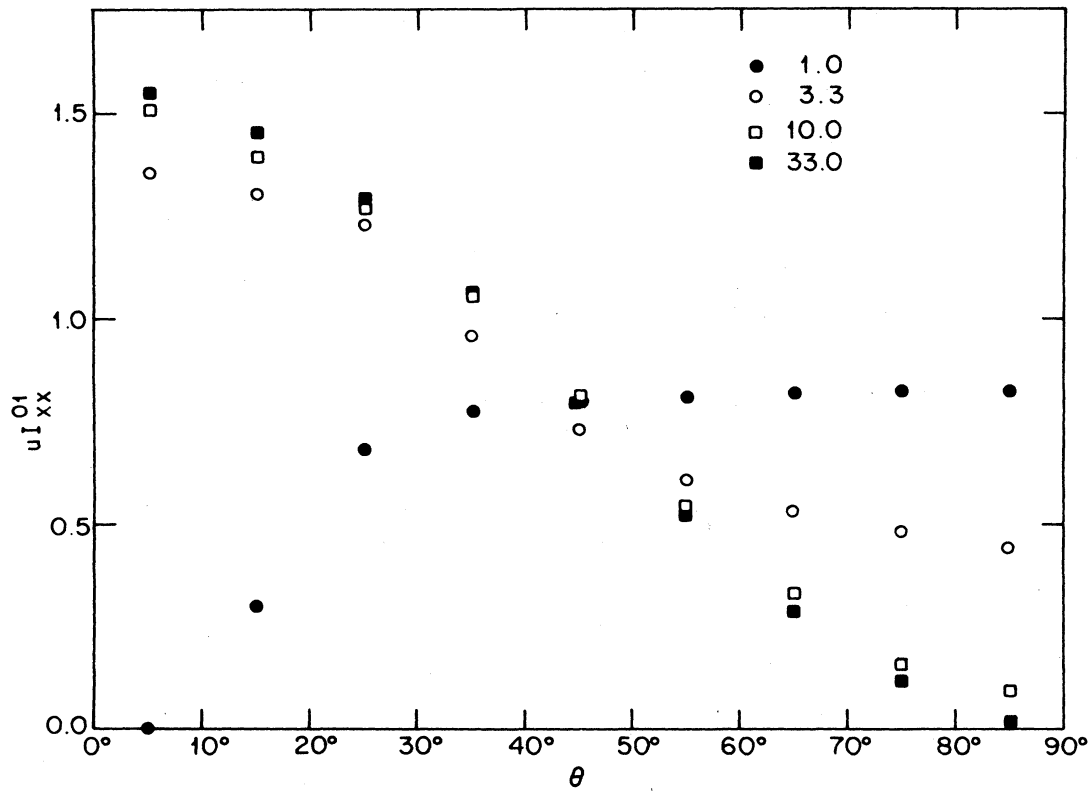


FIG. 11. Plot of the quadratic moment for  $0 \rightarrow 1$  transitions  $I_{xx}^{01}$ , multiplied by  $u$ , as a function of  $\theta$  for four values of  $u$ .

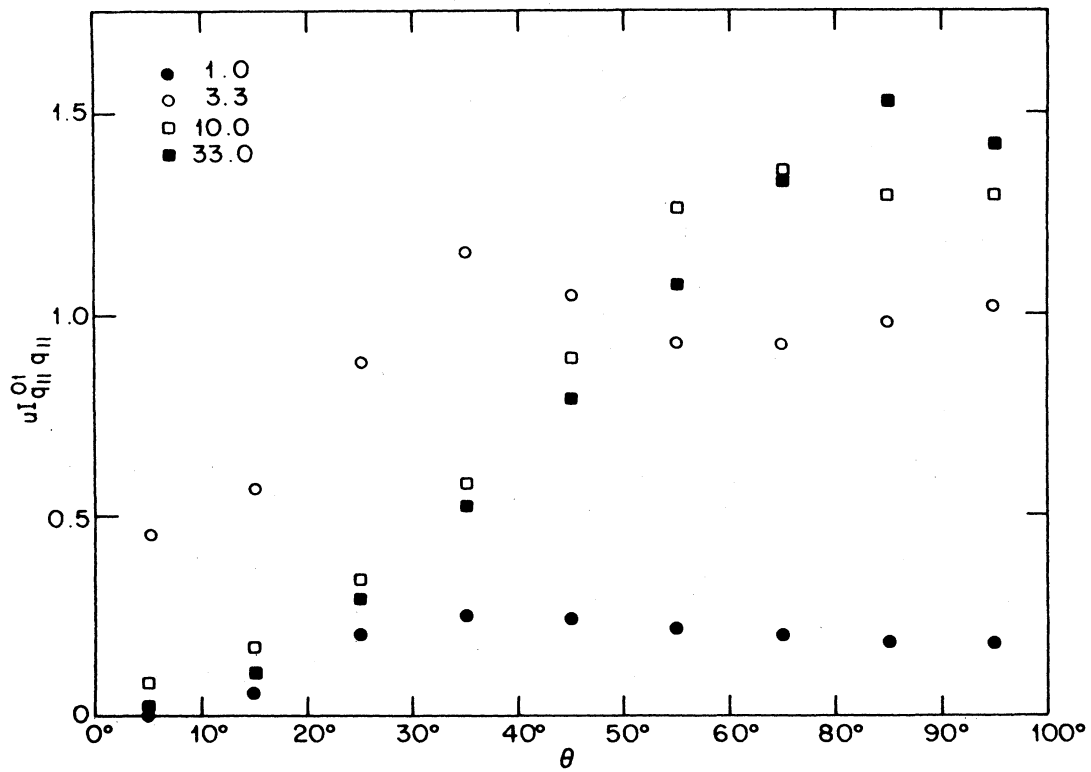


FIG. 12. Plot of the quadratic moment for  $0 \rightarrow 1$  transitions  $I_{q_{||} q_{||}}^{01}$ , multiplied by  $u$ , as a function of  $\theta$  for four values of  $u$ .

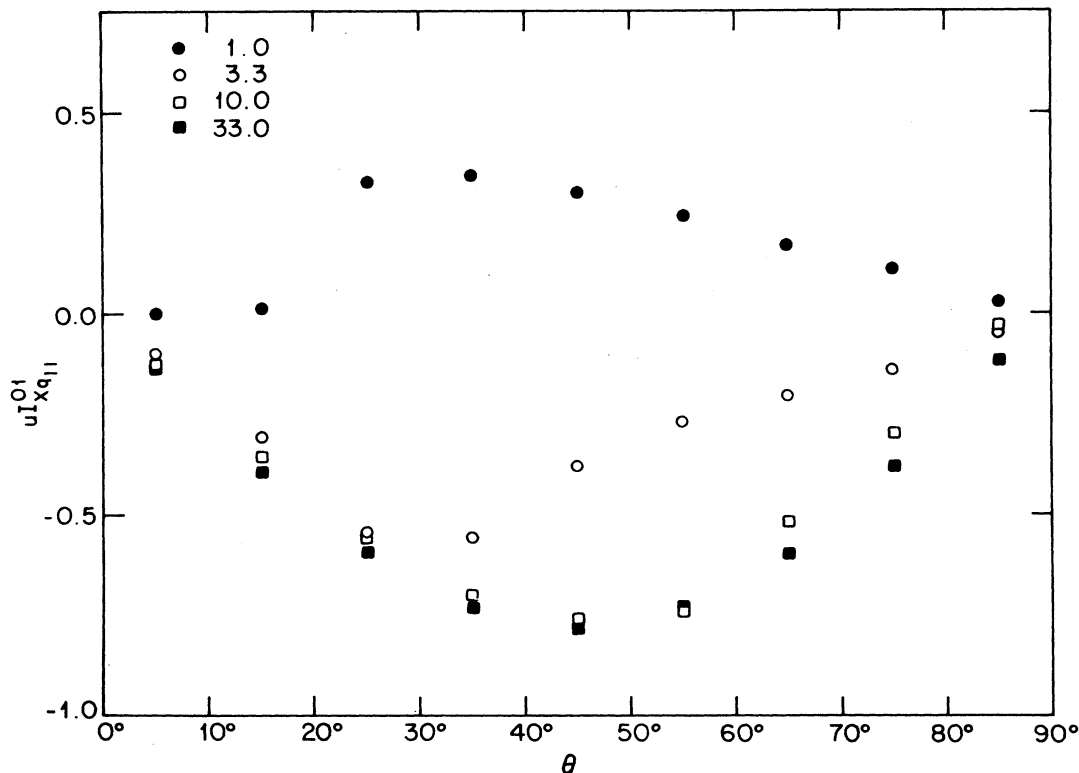


FIG. 13. Plot of the quadratic moment for  $0 \rightarrow 1$  transitions  $I_{xq||}^{01}$ , multiplied by  $u$ , as a function of  $\theta$  for four values of  $u$ .

$$I_{\text{new}}(u, \theta) = \int_{-\infty}^{\infty} f(k_{z,i}) I_{\text{old}}(u', \theta') dk_{z,i},$$

where  $f$  is the electron distribution function and  $I_{\text{old}}$  is the tabulated moment. The arguments  $u'$  and  $\theta'$  are

$$u' = (u^2 - 2uk_{i,z} \cos \theta + k_{i,k}^2)^{1/2},$$

$$\theta' = \tan^{-1}[(u \sin \theta) / (u \cos \theta - k_{i,z})].$$

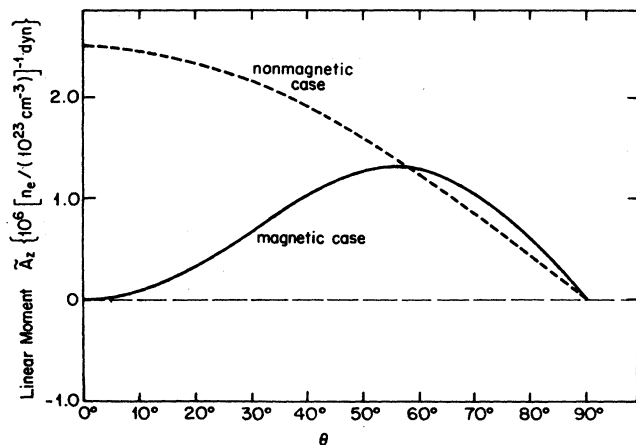


FIG. 14. Drag moment  $\tilde{A}_z$  is graphed in the magnetic ( $B = 10^{12}$  G) and nonmagnetic cases, for a proton traveling at  $0.5c$  with an angle  $\theta$  to the  $z$  axis, through a "cold" plasma (colliding electrons initially at rest) with screening length  $2.6 \times 10^{-7}$  cm, scaled to  $n_e = 10^{23} \text{ cm}^{-3}$ .

In simulations of an atmosphere, the tables provided will be inadequate if a significant fraction of atmospheric electrons contribute values of  $u'$  smaller than those for which the moments were tabulated. This would be the case for a proton moving along the field with a velocity less than or of the order of a typical electron velocity. Such a case is not expected to be of importance in actual simulations, though, as the infalling protons are expected to veer to large pitch angles before decelerating much.

The form in which the data have been presented seems to us the most generally useful, as it is applicable to nonthermal distributions for the atmospheric electrons as well as thermal distributions. In addition, in a Monte Carlo calculation of the stopping length and related problems, one may forego the integration above by merely picking colliding electrons at random from their posited distribution.<sup>24</sup>

A remark on the excitation rate integral ( $I^{01}$ ) is in order. When the proton pitch angle  $\theta \neq 0$ , this integral is nonzero for proton velocities quite a bit less than  $u = \sqrt{2}$ , the threshold for excitation at  $\theta \equiv 0$ . This may be attributed to the fact that only momentum along the field is conserved in a collision. The resonance peak is therefore confined to pitch angles near zero, and is also limited to a very small range of velocities. Figure 7 provides an overview of the excitation rate as a function of proton velocity and pitch angle.

For comparison with our results, the analogous moments for a cold plasma with no magnetic field have been derived and are supplied in Appendix A. Figures 14–16

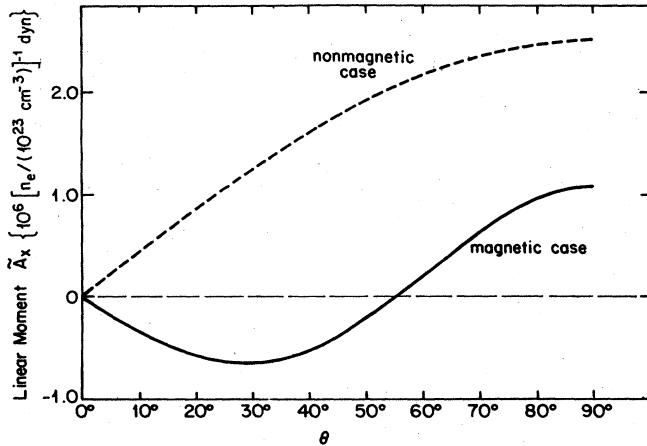


FIG. 15. Drag moment  $\tilde{A}_x$  is graphed in the magnetic ( $B=10^{12}$  G) and nonmagnetic cases, for a proton traveling at  $0.5c$  with an angle  $\theta$  to the  $z$  axis, through a cold plasma with screening length  $2.6 \times 10^{-7}$  cm, scaled to  $n_e = 10^{23} \text{ cm}^{-3}$ .

compare linear moments in the magnetic and nonmagnetic cases for a physically interesting velocity,  $V=0.5c \approx V_{ff}$ . In the magnetic case we have taken  $B=10^{12}$  G. In Fig. 17 we make a similar comparison between the traces of the tensor of quadratic moments in the two cases.

We tested our numerical integrations in several ways. First, we used our routine to evaluate analytically known integrals which in crucial respects (sharp peaking, exponential decay, etc.) resemble our integrals. We also used low-angle approximations to check the accuracy of our numerical results, generally finding agreement to  $\leq 1\%$ . For  $\theta \rightarrow \pi/2$  our approximations (see Appendix B) are rough, and one can only expect order of magnitude agreement with the full numerical results. For  $I_x^{00}$  at high angles, however, one finds agreement within 15%. The approximations in this regime generally do not take proper account of the exponential damping and were not expect-

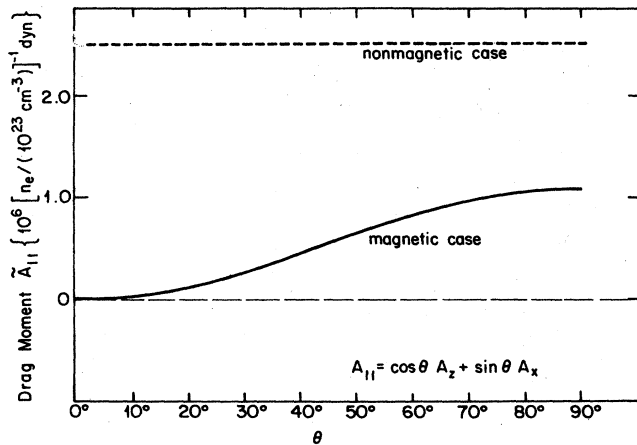


FIG. 16. Drag moment  $\tilde{A}_{||}$  is graphed in the magnetic ( $B=10^{12}$  G) and nonmagnetic cases, for a proton traveling at  $0.5c$  with an angle  $\theta$  to the  $z$  axis, through a cold plasma with screening length  $2.6 \times 10^{-7}$  cm, scaled to  $n_e = 10^{23} \text{ cm}^{-3}$ .

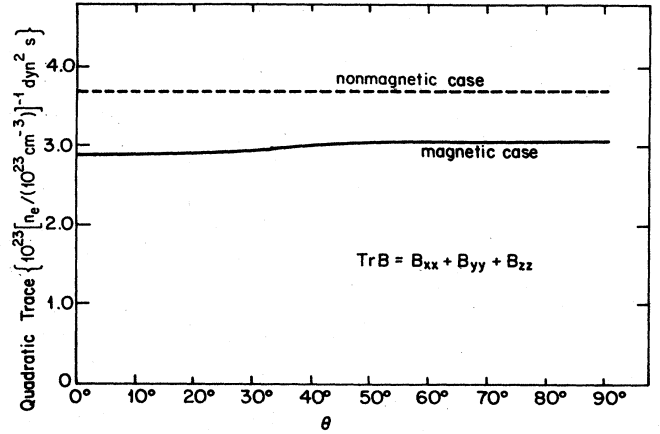


FIG. 17. Trace of the  $V, \theta$  contributions to the Fokker-Planck diffusion tensor  $B_{\alpha\alpha}$  is graphed in the magnetic ( $B=10^{12}$  G) and nonmagnetic cases, for a proton traveling at  $0.5c$  with an angle  $\theta$  to the  $z$  axis, through a cold plasma with screening length  $2.6 \times 10^{-7}$  cm, scaled to  $n_e = 10^{23} \text{ cm}^{-3}$ .

ed to be as successful as the low-angle ones; we cautiously took the agreement of  $I_x^{00}$  as a further indication that the integrals were being done correctly. Another check involved the independent determination of integrals using our "standard" routine, which integrates in  $x$  and  $y$ , and our high-angle routine using  $q_{||}$  and  $y$ . On a sporadic basis, integrals were evaluated without the elaborate subdivision of the integration domain described above, leading to good agreement with the numerical results obtained more efficiently with our standard techniques. Overall, we estimate our numerical accuracy to be better than a few percent.

#### APPENDIX A: CONVERSION TO CONVENTIONAL UNITS

To turn our numbers into quantities in conventional units, note the following.

(i) The transition rate from the lowest to the first excited Landau level is given by

$$\Gamma_{0 \rightarrow 1} = 4\alpha_e^2 (B/B_c)^{-3/2} n_e \frac{\hbar^2}{m_e^2 c} I^{01}.$$

(ii) The contributions by  $0 \rightarrow n'$  transitions with relative (dimensionless) velocity  $u$ , pitch angle  $\theta$ , to the Fokker-Planck drag and diffusion coefficients as defined by Lifshitz and Pitaevskii (Ref. 20, p. 90), are, respectively,

$$\tilde{A}_\beta = 4\alpha_e^2 (B/B_c)^{-1} n_e \frac{\hbar^2}{m_e} I_\beta^{0n'}(u, \theta),$$

$$B_{\beta\gamma} = 2\alpha_e^2 (B/B_c)^{-1/2} n_e \hbar^2 c I_{\beta\gamma}^{0n'}(u, \theta).$$

In the nonmagnetic case we find, for speed  $V$ ,

$$\tilde{A}_\beta = 4\alpha_e^2 n_e \frac{\hbar^2}{m_e} I_\beta(V, \theta) \quad (B=0),$$

$$B_{\beta\gamma} = 2\alpha_e^2 n_e \hbar^2 c I_{\beta\gamma}(V, \theta) \quad (B=0),$$

where

$$\begin{aligned}
 I_x &= \pi \left[ \frac{V}{c} \right]^{-2} \sin\theta (\ln 2 - \ln \zeta - \frac{1}{2}) \quad (B=0), \\
 I_z &= \pi \left[ \frac{V}{c} \right]^{-2} \cos\theta (\ln 2 - \ln \zeta - \frac{1}{2}) \quad (B=0), \\
 I_{xx} &= \pi \left[ \frac{V}{c} \right]^{-1} [\sin^2\theta + \cos^2\theta (\ln 2 - \ln \zeta - 1)] \quad (B=0), \\
 I_{xz} &= \pi \left[ \frac{V}{c} \right]^{-1} \sin\theta \cos\theta (\ln 2 - \ln \zeta) \quad (B=0), \\
 I_{zz} &= \pi \left[ \frac{V}{c} \right]^{-1} [\cos^2\theta + \sin^2\theta (\ln 2 - \ln \zeta - 1)] \quad (B=0), \\
 I_{yy} &= \pi \left[ \frac{V}{c} \right]^{-1} (\ln 2 - \ln \zeta - 1) \quad (B=0)
 \end{aligned}$$

( $\zeta = \hbar k_D / m_e V$ ;  $k_D$  is the Debye wave number).

#### APPENDIX B: ESTIMATES OF THE INTEGRALS IN SOME LIMITING REGIMES

The subscript  $\pm$  in the following results indicates the result for the  $\pm$  channel of the given integral. The total values of the various integrated moments are always sums of contributions from these two channels [see Eqs. (18)–(22)].

For  $\theta \ll 1$ ,  $u \gg 1$  we have approximately

$$\begin{aligned}
 (I_x^{00})_- &\approx \frac{\pi\theta}{u^2} (0.44 + \ln \kappa_s), \\
 (I_{q_{||}}^{00})_- &\approx -\frac{3\pi}{2u^2} \theta^2 (0.44 + \ln \kappa_s) - \frac{\pi}{u^2} \frac{m_e}{m_p} (0.44 + \ln \kappa_s), \\
 (I_{xx}^{00})_- &\approx -\frac{\pi}{u} (0.44 + \ln \kappa_s), \\
 (I_{q_{||}q_{||}}^{00})_- &\approx -\frac{\pi}{u} \theta^2 (0.44 + \ln \kappa_s),
 \end{aligned}$$

$$(I_{q_{||}x}^{00})_- \approx \frac{\pi\theta}{u} (0.44 + \ln \kappa_s),$$

$$(I_{yy}^{00})_- \approx -\frac{\pi}{u} (0.44 + \ln \kappa_s),$$

$$(I_{q_{||}}^{00})_+ \approx \pi \left[ \frac{1}{A} - e^A E_1(A) \right],$$

$$A \equiv 2u^2, \quad E_1(A) = \int_A^\infty \frac{e^{-t}}{t} dt,$$

$$(I_{q_{||}q_{||}}^{00})_+ \approx 2\pi u \left[ \frac{1}{A} - e^A E_1(A) \right].$$

For  $\theta=0$ ,  $u \gg 1$  we have approximately

$$(I_x^{01})_- \approx \frac{\pi}{2u} \left[ \left[ 1 + \frac{B}{2} \right] e^{B/2} E_1 \left[ \frac{B}{2} \right] - 1 \right], \quad B \equiv u^{-2} + \kappa_s^2$$

$$(I_{q_{||}}^{01})_- \approx \frac{(I_x^{01})_-}{u}.$$

For  $\theta \ll 1$ ,  $u \gg 1$  we have approximately

$$(I_x^{01})_- \approx -\frac{\pi\theta}{2u^2} (1 + B \ln B),$$

$$(I_{xx}^{01})_- \approx \frac{\pi}{2u} (1 + B \ln B),$$

$$(I_{q_{||}q_{||}}^{01})_- \approx \frac{-\pi(0.88 + \ln B)}{2u^3},$$

$$(I_{yy}^{01})_- \approx (I_{xx}^{01})_-.$$

For  $\theta = \pi/2 - \phi$ ,  $\phi \ll 1$  we have approximately (accurate only to  $\sim 15\%$ , since the exponential damping in the original integrals was not properly accounted for in the approximations)

$$I_x^{00} \approx -\frac{\pi}{2u^2} (\ln \kappa_s),$$

$$(I_{q_{||}}^{00}) \approx -\frac{3\pi\phi}{2u^2} (\ln \kappa_s - \frac{1}{2} \ln u),$$

$$(I_{yy}^{00}) \approx -\frac{\pi}{u} (\ln \kappa_s).$$

<sup>1</sup>Ya. B. Zeldovich and N. I. Shakura, *Astron. Zh.* **46**, 225 (1969) [*Sov. Astron.* **13**, 175 (1969)].

<sup>2</sup>M. L. Alme and J. R. Wilson, *Astrophys. J.* **186**, 1015 (1973).

<sup>3</sup>S. L. Shapiro and E. E. Salpeter, *Astrophys. J.* **198**, 671 (1975).

<sup>4</sup>J. Trümper *et al.*, *Ann. NY Acad. Sci.* **302**, 538 (1977).

<sup>5</sup>J. Trümper *et al.*, *Astrophys. J. Lett.* **219**, L105 (1978).

<sup>6</sup>M. J. Coe *et al.*, *Nature* **268**, 508 (1977).

<sup>7</sup>W. A. Wheaton *et al.*, *Nature* **282**, 240 (1979).

<sup>8</sup>W. Voges *et al.*, *Astrophys. J.* **263**, 803 (1982).

<sup>9</sup>See S. H. Langer and S. Rappaport, *Astrophys. J.* **257**, 733 (1982) for the discussion of the collisionless shock scenario with  $B \neq 0$ .

<sup>10</sup>M. M. Basko and R. A. Sunyaev, *Zh. Eksp. Teor. Fiz.* **68**, 105 (1975) [*Sov. Phys.—JETP* **41**, 52 (1975)] have also considered

the role of elastic p-p nuclear collisions, which we do not treat here.

<sup>11</sup>J. Ventura, *Phys. Rev. A* **8**, 3021 (1973).

<sup>12</sup>See Ventura (Ref. 11), Basko and Sunyaev (Ref. 10), Kirk and Galloway (Ref. 13). See also G. G. Pavlov and D. G. Yakovlev, *Zh. Eksp. Teor. Fiz.* **70**, 753 (1976) [*Sov. Phys.—JETP* **43**, 389 (1976)]; R. W. Bussard, *Astrophys. J.* **237**, 970 (1980); S. H. Langer, *Phys. Rev. D* **23**, 328 (1981), and references therein.

<sup>13</sup>J. G. Kirk and D. J. Galloway, *Plasma Phys.* **24**, 339 (1982); *Mon. Not. R. Astron. Soc.* **195**, 45P (1981).

<sup>14</sup>M. H. Johnson and B. A. Lippman, *Phys. Rev.* **76**, 828 (1949).

<sup>15</sup>S. L. Shapiro and S. A. Teukolsky, *Black Holes, White Dwarfs, and Neutron Stars* (Wiley, New York, 1983).

- <sup>16</sup>S. H. Langer (unpublished).
- <sup>17</sup>R. N. Manchester and J. H. Taylor, *Pulsars* (Freeman, San Francisco, 1977).
- <sup>18</sup>N. Horing, *Ann. Phys.* **54**, 405 (1969).
- <sup>19</sup>S. Ichimaru, *Basic Principles in Plasma Physics* (Benjamin, Reading, 1973).
- <sup>20</sup>E. M. Lifshitz and L. P. Pitaevskii, *Physical Kinetics* (Pergamon, Oxford, 1981).
- <sup>21</sup>I. S. Gradshteyn and I. M. Ryzhik, *Table of Integrals, Series, and Products* (Academic, New York, 1980).
- <sup>22</sup>V. Canuto and J. Ventura, *Fundam. Cosmic Phys.* **2**, 203 (1977).
- <sup>23</sup>See AIP document No. PAPS PLRAAH-31-120-27 for 27 pages of numerical data corresponding to Tables 1–10. Order by PAPS number and journal reference from American Institute of Physics, Physics Auxiliary Publication Service, 335 East 45th Street, New York, NY 10017. The prepaid price is \$1.50 for a microfiche, or \$5.00 for a photocopy. Airmail additional.
- <sup>24</sup>G. Miller, E. E. Salpeter, and I. Wasserman (unpublished).